STEADY-STATE ANALYSIS AND DESIGN METHODOLOGY FOR CLASS-E^2 RESONANT DC/DC CONVERTERS BASED ON A NORMALIZED STATE-SPACE MODEL

Lucas S. Mendonça[1], João Pedro S. Cipriani[1] and Thiago C. Naidon[1] and Fábio E. Bisogno[1]
[1]Universidade Federal de Santa Maria, Santa Maria (UFSM) – Rio Grande do Sul, Brazil
e-mail: lucassangoi1993@gmail.com

***Abstract* – This paper presents a steady-state analysis and design methodology for the Class-E^2 resonant DC/DC converter. The converter is represented in a normalized state-space model that is independent of specifications and real system components, like as inductors, capacitors and resistors. Analytical waveforms are obtained and can be used to design the converter. The main contribution of the paper is the development of an analysis methodology that does not separate the inverter and rectifier stages and ensures the soft-switching on both switch and diode. A step-by-step design procedure is presented, in which the real system components can be obtained based on design abacus. A comparison among theoretical, simulation and experimental results are performed based on a design example.**

***Keywords* – Circuit Analysis, Resonant Power Conversion, State-Space Methods.**

I. INTRODUCTION

By cascading a resonant DC/AC inverter to a resonant AC/DC rectifier, a resonant DC/DC converter is obtained [1]. This type of topology can be used as an electrical model for systems supplied by a DC input providing an DC output and concomitantly including an AC power conversion stage.

Resonant power converters are suitable when AC waveforms are required in applications like as wireless power transfer (WPT) [2]–[4], low power sensor nodes [5], [6], energy harvesting systems [7], [8] and so on. Usually, resonant DC/AC inverters can be used to supply piezoelectric transformers [9], [10], the primary side of WPT systems [11], [12] and ultrasonic transducers. Some resonant AC/DC rectifier applications can be founded for low power energy harvesting and lighting systems [13], [14]. In all instances, the motivation behind is to perform the soft-switching conditions: zero-voltage (ZVS), zero-current (ZCS) and zero-derivative (ZDS) switching, which make possible to reduce switching losses and increase the operating frequency [15]–[19].

Considering DC/DC resonant converters, Class-D, Class-E, Half/Full-bridge with resonant tanks are commonly used for the inverter stage. Full-bridge topologies achieve higher transfer power ratio. On the other hand, the Class-E resonant inverter has the advantage that only one switch is used. When the Class-E resonant inverter and the Class-E resonant rectifier are connected in series, the Class-E^2 resonant DC/DC converter is obtained as depicted in Figure 1, composed by: inductor L_f, resonant tank L_r-C_r, capacitor C_1, switch S, capacitor C_2, diode D, output filter L_f-C_f and load R_L. The Class-E^2 converter operates at ZVS and ZDS conditions. When the switch S turns on, its voltage is zero; when the diode D turns off, its voltage is zero and the derivative of its voltage is zero. However, in order to achieve such optimal steady-state operation, it is necessary to obtain analytical waveforms, which have high mathematical complexity. Most of previous researches of the Class-E^2 resonant converter analyze the topology by separating the inverter and the rectifier stages [12], [15], [21]–[23]. This simplification can be used to design the converter, however, it is necessary to ensure the both stages are compatible with each other.

In this sense, this works present a steady-state analysis methodology, in which the analytical waveforms of the Class-E^2 resonant converter are obtained by considering the converter as only one combined circuit. It is specially challenging to solve the forth operating mode of the converter, in which the switch S and the diode D are off. It is because a circuit composed by four reactive elements C_1-L_r-C_r-C_2 is retrieved. For this purpose, a normalized state-space model is used to represent the converter, in which the system becomes independently of specifications like as input/output voltage, power and operating frequency; and real system parameters such as inductors, capacitors and resistors. By representing the converter by means of the resonant frequencies among the reactive components, it is possible to obtain the analytical waveforms ensuring the soft-switching conditions for any reasonable operating point. A step-by-step design procedure, in which by defining design specifications and selecting an operating point, the converter can be easily designed by means of normalized gain curves (design abacus) is presented as contribution. The proposed method is more suitable when it is necessary to design the converter without separating the inverter and the rectifier stages. The theoretical results are validate by means of simulation and experimental results.

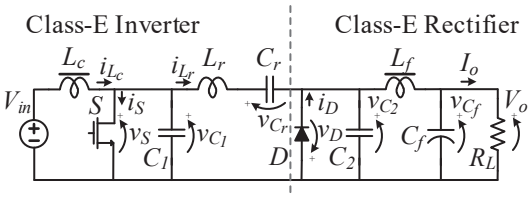

Fig. 1. Class-E^2 resonant DC/DC converter.

Manuscript received 01/08/2020; first revision 04/21/2020; accepted for publication 06/25/2020, by recommendation of Editor Demercil de Souza Oliveira Jr.. http://dx.doi.org/10.18618/REP.2020.2.0002

II. MATHEMATICAL APPROACH

The main features of the Class-E^2 resonant DC/DC converter are the switch S zero-voltage switching and the diode D zero-derivative voltage switching. In this sense, the proposed modeling approach is going to be conducted by considering the following assumptions:

1. The input voltage source V_{in} and the input choke inductor L_c are replaced by a constant current source I_{in};
2. The output filter L_f-C_f and the load R_L are replaced by a constant current source I_o;
3. The switch S and diode D off states are modeled as a open circuit;
4. The switch S and diode D on states are modeled as a short-circuit.

The model for the converter is portrayed in Figure 2:

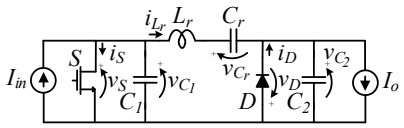

Fig. 2. Class-E^2 resonant DC/DC converter model.

The converter has four operating modes that are depicted in Figures 3.a-3.d. The resonant capacitor C_r is ruled by the following differential equation at any operating mode:

$$\frac{dv_{C_r}(t)}{dt} = \frac{i_{L_r}(t)}{C_r}. \tag{1}$$

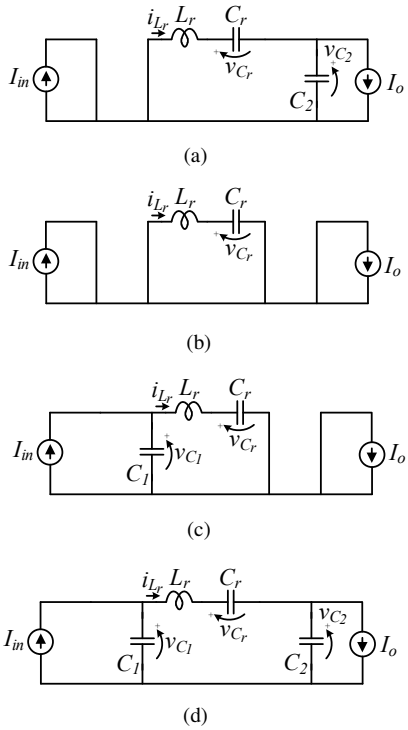

Fig. 3. Operating modes. (a) Switch S on and diode D off. (b) Switch S on and diode D on. (c) Switch S off and diode D on. (d) Switch S off and diode D off.

At mode I ($0 < t \leq T_1$): *S on* and *D off*. The converter is ruled by the following differential equations:

$$\frac{di_{L_r}(t)}{dt} = -\frac{v_{C_r}(t)}{L_r} - \frac{v_{C_2}(t)}{L_r}, \tag{2}$$

$$\frac{dv_{C_1}(t)}{dt} = 0 \tag{3}$$

and

$$\frac{dv_{C_2}(t)}{dt} = \frac{i_{L_r}(t)}{C_2} - \frac{I_o}{C_2}. \tag{4}$$

At mode II ($T_1 < t \leq D_c 2\pi$): *S on* and *D on*. The following equations are considered:

$$\frac{di_{L_r}(t)}{dt} = -\frac{v_{C_r}(t)}{L_r}, \tag{5}$$

$$\frac{dv_{C_1}(t)}{dt} = 0 \tag{6}$$

and

$$\frac{dv_{C_2}(t)}{dt} = 0. \tag{7}$$

At mode III ($D_c 2\pi < t \leq T_2$): *S off* and *D on*. The converter is governed by:

$$\frac{di_{L_r}(t)}{dt} = \frac{v_{C_1}(t)}{L_r} - \frac{v_{C_r}(t)}{L_r}, \tag{8}$$

$$\frac{dv_{C_1}(t)}{dt} = \frac{I_{in}}{C_1} - \frac{i_{L_r}(t)}{C_1} \tag{9}$$

and

$$\frac{dv_{C_2}(t)}{dt} = 0. \tag{10}$$

At mode IV ($T_2 < t \leq 2\pi$): *S off* and *D off*. The differential equations are:

$$\frac{di_{L_r}(t)}{dt} = \frac{v_{C_1}(t)}{L_r} - \frac{v_{C_r}(t)}{L_r} - \frac{v_{C_2}(t)}{L_r}, \tag{11}$$

$$\frac{dv_{C_1}(t)}{dt} = \frac{I_{in}}{C_1} - \frac{i_{L_r}(t)}{C_1} \tag{12}$$

and

$$\frac{dv_{C_2}(t)}{dt} = \frac{i_{L_r}(t)}{C_2} - \frac{I_o}{C_2}. \tag{13}$$

The system is represented by a state-space model as follows, in which i is the index for the converter operating mode and it is described by: state matrix $\mathbf{A}_i$, input matrix $\mathbf{B}_i$, output matrix $\mathbf{C}_i$ and transmission matrix $\mathbf{D}_i$:

$$\mathbf{x}(t) = \mathbf{A}_i\mathbf{x}(t) + \mathbf{B}_i\mathbf{u}(t) \tag{14}$$

and

$$\mathbf{y}(t) = \mathbf{C}_i\mathbf{x}(t) + \mathbf{D}_i\mathbf{u}(t), \tag{15}$$

in which, the state vector $\mathbf{x}(t)$, output vector $\mathbf{y}(t)$ and input vector $\mathbf{u}(t)$ are written as:

$$\mathbf{x}(t) = \left[\mathbf{i_{L_r}}, \mathbf{v_{C_r}}, \mathbf{v_{C_1}}, \mathbf{v_{C_2}}\right]^T, \tag{16}$$

$$\mathbf{y}(t) = \left[\frac{\mathbf{i_{L_r}}}{\mathbf{I_{in}}}, \frac{\mathbf{v_{C_r}}}{\mathbf{V_{in}}}, \frac{\mathbf{v_{C_1}}}{\mathbf{V_{in}}}, \frac{\mathbf{v_{C_2}}}{\mathbf{V_{in}}}, \frac{\mathbf{i_S}}{\mathbf{I_{in}}}, \frac{\mathbf{i_D}}{\mathbf{I_{in}}}\right]^T \tag{17}$$

and

$$\mathbf{u}(t) = [\mathbf{I_{in}}, \mathbf{I_o}]^T. \tag{18}$$

In (17), the variables are parameterized by the input current I_{in} or the input voltage V_{in}. The input vector variables can be changed by the stored energy in the reactive components. In this sense, a new input vector $\mathbf{x_e}(t)$ is selected as [20]:

$$\mathbf{x_e}(t) = \left[\mathbf{i_{L_r}}\frac{\sqrt{\mathbf{L_r}}}{\sqrt{\mathbf{2}}}, \mathbf{v_{C_r}}\frac{\sqrt{\mathbf{C_r}}}{\sqrt{\mathbf{2}}}, \mathbf{v_{C_1}}\frac{\sqrt{\mathbf{C_1}}}{\sqrt{\mathbf{2}}}, \mathbf{v_{C_2}}\frac{\sqrt{\mathbf{C_2}}}{\sqrt{\mathbf{2}}}\right]^T, \quad (19)$$

the new input vector is used to perform an equivalence transformation $\mathbf{P}$ as follows:

$$\mathbf{P} = \mathbf{x_e}(t)\cdot\mathbf{x}(t)^{-1}. \quad (20)$$

In (20), $\mathbf{x}(t)$ and $\mathbf{x_e}(t)$ must be evaluated in their diagonal matrices forms. In order to normalize the system in relation to the input current source I_{in} and the operating angular frequency ω, a normalization factor Γ is defined as [20]

$$\Gamma = \frac{\omega}{I_{in}}\sqrt{2C_2}, \quad (21)$$

the new state, input, output and transmission matrices, $\overline{\mathbf{A}_i}$, $\overline{\mathbf{B}_i}$, $\overline{\mathbf{C}_i}$ and $\overline{\mathbf{D}_i}$, respectively and considering the new vector space $\mathbf{x_e}(t)$ are found by [20]:

$$\overline{\mathbf{A}_i} = \frac{\Gamma\mathbf{P}\cdot\mathbf{A}_i\cdot(\Gamma\mathbf{P})^{-1}}{\omega}, \quad (22)$$

$$\overline{\mathbf{B}_i} = \frac{\Gamma\mathbf{P}\cdot\mathbf{B}_i}{\omega}, \quad (23)$$

$$\overline{\mathbf{C}_i} = \frac{\mathbf{C}_i\cdot(\Gamma\mathbf{P})^{-1}}{\omega} \quad (24)$$

and

$$\overline{\mathbf{D}_i} = \mathbf{D}_i, \quad (25)$$

which leads to:

$$\overline{\mathbf{A}_I}=\begin{bmatrix} 0 & \frac{-1}{\sqrt{L_rC_r}} & 0 & \frac{-1}{\sqrt{L_rC_2}} \\ \frac{1}{\sqrt{L_rC_r}} & 0 & 0 & 0 \\ 0 & 0 & 0 & 0 \\ \frac{1}{\sqrt{L_rC_2}} & 0 & 0 & 0 \end{bmatrix}, \quad \overline{\mathbf{B}_I}=\begin{bmatrix} 0 & 0 \\ 0 & 0 \\ 0 & 0 \\ 0 & \frac{-1}{I_{in}} \end{bmatrix},$$

$$\overline{\mathbf{A}_{II}}=\begin{bmatrix} 0 & \frac{-1}{\sqrt{L_rC_r}} & 0 & 0 \\ \frac{1}{\sqrt{L_rC_r}} & 0 & 0 & 0 \\ 0 & 0 & 0 & 0 \\ 0 & 0 & 0 & 0 \end{bmatrix}, \quad \overline{\mathbf{B}_{II}}=\begin{bmatrix} 0 & 0 \\ 0 & 0 \\ 0 & 0 \\ 0 & 0 \end{bmatrix},$$

$$\overline{\mathbf{A}_{III}}=\begin{bmatrix} 0 & \frac{-1}{\sqrt{L_rC_r}} & \frac{1}{\sqrt{L_rC_1}} & 0 \\ \frac{1}{\sqrt{L_rC_r}} & 0 & 0 & 0 \\ \frac{-1}{\sqrt{L_rC_r}} & 0 & 0 & 0 \\ 0 & 0 & 0 & 0 \end{bmatrix}, \quad \overline{\mathbf{B}_{III}}=\begin{bmatrix} 0 & 0 \\ 0 & 0 \\ \frac{\sqrt{C_2}}{\sqrt{C_1}I_{in}} & 0 \\ 0 & 0 \end{bmatrix},$$

$$\overline{\mathbf{A}_{IV}}=\begin{bmatrix} 0 & \frac{-1}{\sqrt{L_rC_r}} & \frac{1}{\sqrt{L_rC_1}} & \frac{-1}{\sqrt{L_rC_2}} \\ \frac{1}{\sqrt{L_rC_r}} & 0 & 0 & 0 \\ \frac{-1}{\sqrt{L_rC_1}} & 0 & 0 & 0 \\ \frac{1}{\sqrt{L_rC_2}} & 0 & 0 & 0 \end{bmatrix}, \overline{\mathbf{B}_{IV}}=\begin{bmatrix} 0 & 0 \\ \frac{\sqrt{C_2}}{\sqrt{C_1}I_{in}} & 0 \\ 0 & 0 \\ 0 & \frac{-1}{I_{in}} \end{bmatrix},$$

$$\overline{\mathbf{C}_I}=\begin{bmatrix} \frac{1}{\sqrt{L_rC_2}} & 0 & 0 & 0 \\ 0 & \frac{I_{in}}{\sqrt{C_rC_2}V_{in}\omega} & 0 & 0 \\ 0 & 0 & \frac{I_{in}}{\sqrt{C_1C_2}V_{in}\omega} & 0 \\ 0 & 0 & 0 & \frac{I_{in}}{C_2V_{in}\omega} \\ -\frac{1}{\sqrt{L_rC_2}\omega} & 0 & 0 & 0 \\ 0 & 0 & 0 & 0 \end{bmatrix},$$

$$\overline{\mathbf{C}_{II}}=\begin{bmatrix} \frac{1}{\sqrt{L_rC_2}} & 0 & 0 & 0 \\ 0 & \frac{I_{in}}{\sqrt{C_rC_2}V_{in}\omega} & 0 & 0 \\ 0 & 0 & \frac{I_{in}}{\sqrt{C_1C_2}V_{in}\omega} & 0 \\ 0 & 0 & 0 & \frac{I_{in}}{C_2V_{in}\omega} \\ -\frac{1}{\sqrt{L_rC_2}\omega} & 0 & 0 & 0 \\ -\frac{1}{\sqrt{L_rC_2}\omega} & 0 & 0 & 0 \end{bmatrix},$$

$$\overline{\mathbf{C}_{III}}=\begin{bmatrix} \frac{1}{\sqrt{L_rC_2}} & 0 & 0 & 0 \\ 0 & \frac{I_{in}}{\sqrt{C_rC_2}V_{in}\omega} & 0 & 0 \\ 0 & 0 & \frac{I_{in}}{\sqrt{C_1C_2}V_{in}\omega} & 0 \\ 0 & 0 & 0 & \frac{I_{in}}{C_2V_{in}\omega} \\ 0 & 0 & 0 & 0 \\ -\frac{1}{\sqrt{L_rC_2}\omega} & 0 & 0 & 0 \end{bmatrix},$$

$$\overline{\mathbf{C}_{IV}}=\begin{bmatrix} \frac{1}{\sqrt{L_rC_2}} & 0 & 0 & 0 \\ 0 & \frac{I_{in}}{\sqrt{C_rC_2}V_{in}\omega} & 0 & 0 \\ 0 & 0 & \frac{I_{in}}{\sqrt{C_1C_2}V_{in}\omega} & 0 \\ 0 & 0 & 0 & \frac{I_{in}}{C_2V_{in}\omega} \\ 0 & 0 & 0 & 0 \\ 0 & 0 & 0 & 0 \end{bmatrix},$$

$$\overline{\mathbf{D}_I}=\begin{bmatrix} 0 & 0 & 0 & 0 & 1/I_{in} & 0 \\ 0 & 0 & 0 & 0 & 0 & 0 \end{bmatrix}^T,$$

$$\overline{\mathbf{D}_{II}}=\begin{bmatrix} 0 & 0 & 0 & 0 & 1/I_{in} & 0 \\ 0 & 0 & 0 & 0 & 0 & 1/I_{in} \end{bmatrix}^T,$$

$$\overline{\mathbf{D}_{III}}=\begin{bmatrix} 0 & 0 & 0 & 0 & 0 & 0 \\ 0 & 0 & 0 & 0 & 0 & 1/I_{in} \end{bmatrix}^T$$

and

$\overline{\mathbf{D}_{IV}}$=0.

The terms in the state matrices can be rewritten as function of unit-less parameters instead of real system parameters, like as L_r, C_r, C_1 and C_2 [24]. Towards this end, the resonant frequencies among the reactive components are used as

$$\omega_1 = \frac{1}{\sqrt{L_rC_1}}; \omega_2 = \frac{1}{\sqrt{L_rC_r}}; \omega_3 = \frac{1}{\sqrt{L_rC_2}}. \quad (26)$$

By normalizing the resonant frequencies by the operating angular frequency, unit-less parameters are achieved as

$$A_1 = \frac{\omega_1}{\omega}; A_2 = \frac{\omega_2}{\omega}; A_3 = \frac{\omega_3}{\omega}. \quad (27)$$

Parameters A_1, A_2 and A_3 are named as normalized resonant frequencies. Other unit-less parameters should be introduced. The quality factor Q_L can be equated as function of the output load R_L by [1]

$$Q_L = \frac{R_L}{\omega_3 L_r} = \omega_3 C_2 R_L. \quad (28)$$

The current transfer function S is defined by the relation between the input and output currents as

$$S = \frac{I_o}{I_{in}}. \tag{29}$$

Furthermore, the input to output relation a can be equated by [24]

$$a = \frac{V_{in}}{I_{in} R_L}. \tag{30}$$

It can be seen that the terms in matrices $\overline{\mathbf{B}_I}$, $\overline{\mathbf{B}_{II}}$, $\overline{\mathbf{B}_{III}}$, $\overline{\mathbf{B}_{IV}}$, $\overline{\mathbf{D}_I}$, $\overline{\mathbf{D}_{II}}$, $\overline{\mathbf{D}_{III}}$ and $\overline{\mathbf{D}_{IV}}$ can be re-positioned into the input vector $\mathbf{u}(t)$ by considering

$$\mathbf{u}(\omega t) = \left[\frac{\mathbf{I_{in}}}{\mathbf{I_{in}}}, \frac{\mathbf{I_o}}{\mathbf{I_{in}}}\right]^T = [1, S]^T = \left[1, \frac{1}{\sqrt{a}}\right]^T. \tag{31}$$

By using (26), (27), (28), (29) and (30), the terms in the state matrices can be replaced by unit-less parameters and a normalized state-space model can be used as mathematical model for the converter as [25]

$$\mathbf{x_e}(\omega t) = \mathbf{E}_{i_{[A_1,A_2,A_3]}} \mathbf{x_e}(\omega t) + \mathbf{F}_{i[A_1,A_3]} \mathbf{u}(\omega t) \tag{32}$$

and

$$\mathbf{y}(\omega t) = \mathbf{G}_{i_{[A_1,A_2,A_3,Q_L,a]}} \mathbf{x_e}(\omega t) + \mathbf{H}_i \mathbf{u}(\omega t), \tag{33}$$

$\mathbf{E}_i$, $\mathbf{F}_i$, $\mathbf{G}_i$ and $\mathbf{H}_i$ are the unit-less state-space matrices, in which

$$\mathbf{E}_I = \begin{bmatrix} 0 & -A_2 & 0 & -A_3 \\ A_2 & 0 & 0 & 0 \\ 0 & 0 & 0 & 0 \\ A_3 & 0 & 0 & 0 \end{bmatrix}, \quad \mathbf{F}_I = \begin{bmatrix} 0 & 0 \\ 0 & 0 \\ 0 & 0 \\ 0 & -1 \end{bmatrix},$$

$$\mathbf{E}_{II} = \begin{bmatrix} 0 & -A_2 & 0 & 0 \\ A_2 & 0 & 0 & 0 \\ 0 & 0 & 0 & 0 \\ 0 & 0 & 0 & 0 \end{bmatrix}, \quad \mathbf{F}_{II} = \begin{bmatrix} 0 & 0 \\ 0 & 0 \\ 0 & 0 \\ 0 & 0 \end{bmatrix},$$

$$\mathbf{E}_{III} = \begin{bmatrix} 0 & -A_2 & A_1 & 0 \\ A_2 & 0 & 0 & 0 \\ -A_1 & 0 & 0 & 0 \\ 0 & 0 & 0 & 0 \end{bmatrix}, \quad \mathbf{F}_{III} = \begin{bmatrix} 0 & 0 \\ 0 & 0 \\ \frac{A_1}{A_3} & 0 \\ 0 & 0 \end{bmatrix},$$

$$\mathbf{E}_{IV} = \begin{bmatrix} 0 & -A_2 & A_1 & -A_3 \\ A_2 & 0 & 0 & 0 \\ -A_1 & 0 & 0 & 0 \\ A_3 & 0 & 0 & 0 \end{bmatrix}, \quad \mathbf{F}_{IV} = \begin{bmatrix} 0 & 0 \\ \frac{A_1}{A_3} & 0 \\ 0 & 0 \\ 0 & -1 \end{bmatrix},$$

$$\mathbf{G}_I = \begin{bmatrix} A_3 & 0 & 0 & 0 \\ 0 & \frac{A_2}{aQ_L} & 0 & 0 \\ 0 & 0 & \frac{A_1}{aQ_L} & 0 \\ 0 & 0 & 0 & \frac{A_3}{aQ_L} \\ -A_3 & 0 & 0 & 0 \\ 0 & 0 & 0 & 0 \end{bmatrix}, \quad \mathbf{H}_I = \begin{bmatrix} 0 & 0 \\ 0 & 0 \\ 0 & 0 \\ 0 & 0 \\ 1 & 0 \\ 0 & 0 \end{bmatrix},$$

$$\mathbf{G}_{II} = \begin{bmatrix} A_3 & 0 & 0 & 0 \\ 0 & \frac{A_2}{aQ_L} & 0 & 0 \\ 0 & 0 & \frac{A_1}{aQ_L} & 0 \\ 0 & 0 & 0 & \frac{A_3}{aQ_L} \\ -A_3 & 0 & 0 & 0 \\ -A_3 & 0 & 0 & 0 \end{bmatrix}, \quad \mathbf{H}_{II} = \begin{bmatrix} 0 & 0 \\ 0 & 0 \\ 0 & 0 \\ 0 & 0 \\ 1 & 0 \\ 0 & 1 \end{bmatrix},$$

$$\mathbf{G}_{III} = \begin{bmatrix} A_3 & 0 & 0 & 0 \\ 0 & \frac{A_2}{aQ_L} & 0 & 0 \\ 0 & 0 & \frac{A_1}{aQ_L} & 0 \\ 0 & 0 & 0 & \frac{A_3}{aQ_L} \\ 0 & 0 & 0 & 0 \\ -A_3 & 0 & 0 & 0 \end{bmatrix}, \quad \mathbf{H}_{III} = \begin{bmatrix} 0 & 0 \\ 0 & 0 \\ 0 & 0 \\ 0 & 0 \\ 0 & 0 \\ 0 & 0 \end{bmatrix},$$

$$\mathbf{G}_{IV} = \begin{bmatrix} A_3 & 0 & 0 & 0 \\ 0 & \frac{A_2}{aQ_L} & 0 & 0 \\ 0 & 0 & \frac{A_1}{aQ_L} & 0 \\ 0 & 0 & 0 & \frac{A_3}{aQ_L} \\ 0 & 0 & 0 & 0 \\ 0 & 0 & 0 & 0 \end{bmatrix} \text{ and } \mathbf{H}_{IV} = 0.$$

By symbolically solving the state-space representation for each operating mode ($i = I, II, III, IV$), steady-state solutions can be achieved. An algorithm is proposed to solve the system, depicted as a flowchart in Figure 4. For the flowchart, the dotted lines represent the outputs and the continuous lines the changes of states defined by the operation related to S and D.

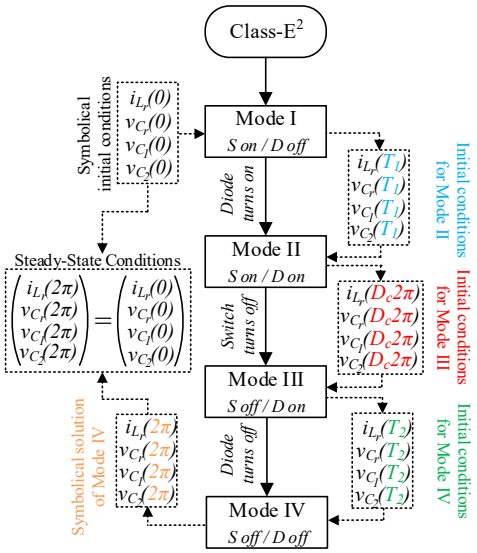

Fig. 4. Flowchart to solve the Class-E^2 resonant DC/DC converter model.

In order to solve mode I, symbolical initial conditions are used as: initial resonant inductor current $i_{L_r}(0)$, initial resonant capacitor voltage $v_{C_r}(0)$, initial capacitor C_1 voltage $v_{C_1}(0)$ and initial rectifier capacitor C_2 voltage $v_{C_2}(0)$. By solving mode I, one equation for each state variable is found, which are dependent of the unit-less parameters and as function of ωt. By replacing ωt by T_1, which represents the end of mode I, the initial conditions to solve mode II are achieved and can be described by $i_{L_r}(T_1)$, $v_{C_r}(T_1)$, $v_{C_1}(T_1)$ and $v_{C_2}(T_2)$. By solving mode II and replacing ωt by $D_c 2\pi$, which characterizes the end of mode II, the initial conditions for mode III are set as $i_{L_r}(D_c 2\pi)$, $v_{C_r}(D_c 2\pi)$, $v_{C_1}(D_c 2\pi)$ and $v_{C_2}(D_c 2\pi)$. The same concept is used for mode III, which ends at T_2, being $i_{L_r}(T_2)$, $v_{C_r}(T_2)$, $v_{C_1}(T_2)$ and $v_{C_2}(T_2)$ the initial conditions to solve mode IV. The last operating mode ends at 2π, which leads to the final conditions described as $i_{L_r}(2\pi)$, $v_{C_r}(2\pi)$, $v_{C_1}(2\pi)$ and $v_{C_2}(2\pi)$. The aforementioned symbolical solutions are dependent of nine parameters A_1, A_2, A_3, a, D_c, $i_{L_r}(0)$, $v_{C_r}(0)$,

$v_{C_1}(0)$ and $v_{C_2}(0)$. By equating the final conditions as equal to the initial conditions (steady-state condition), a linear system composed by four equations can be evaluated. In order to ensure the soft-switching operation of both switch S and diode D, the zero-voltage switching conditions must be addressed to the linear system. When the switch S turns on at 2π, the capacitor C_1 voltage is 0 and the input current I_{in} is equal to the resonant current i_{L_r}. When the diode turns off at T_3, the capacitor C_2 voltage and its derivative are 0. The following steady-state and soft-switching conditions are considered:

- $i_{L_r}(2\pi) = i_{L_r}(0)$ (steady-state condition);
- $v_{C_r}(2\pi) = v_{C_r}(0)$ (steady-state condition);
- $v_{C_1}(2\pi) = 0$ (switch S ZVS condition);
- $v_{C_2}(2\pi) = v_{C_2}(0)$ (steady-state condition);
- $i_{L_r}(2\pi) = I_{in}$ (switch S ZVS condition);
- $v_{C_2}(T_3) = 0$ (diode D ZDVS condition);
- $i_{L_r}(T_3) = I_o$ (diode D ZDVS condition).

The inherent system condition for capacitor C_1 voltage simplifies the linear system by equating $v_{C_1}(0) = 0$. Based on that, the following linear system is equated:

$$\begin{pmatrix} i_{L_r}(2\pi)_{[A_1,A_2,A_3,i_{L_r}(0),v_{C_r}(0),v_{C_2}(0),D_c,T_1,T_2,a]} \\ v_{C_r}(2\pi)_{[A_1,A_2,A_3,i_{L_r}(0),v_{C_r}(0),v_{C_2}(0),D_c,T_1,T_2,a]} \\ v_{C_1}(2\pi)_{[A_1,A_2,A_3,i_{L_r}(0),v_{C_r}(0),v_{C_2}(0),D_c,T_1,T_2,a]} \\ v_{C_2}(2\pi)_{[A_1,A_2,A_3,i_{L_r}(0),v_{C_r}(0),v_{C_2}(0),D_c,T_1,T_2,a]} \\ i_{L_r}(2\pi)_{[A_1,A_2,A_3,i_{L_r}(0),v_{C_r}(0),v_{C_2}(0),D_c,T_1,T_2,a]} \\ v_{C_2}(T_3)_{[A_1,A_2,A_3,i_{L_r}(0),v_{C_r}(0),v_{C_2}(0),D_c,T_1,T_2,a]} \\ i_{L_r}(T_3)_{[A_1,A_2,A_3,i_{L_r}(0),v_{C_r}(0),v_{C_2}(0),D_c,T_1,T_2,a]} \end{pmatrix} = \begin{pmatrix} i_{L_r}(0) \\ v_{C_r}(0) \\ 0 \\ v_{C_2}(0) \\ \frac{1}{A_3} \\ 0 \\ \frac{1}{A_3\sqrt{a}} \end{pmatrix} \tag{34}$$

Note that the diode turn-on and turn off are consequences of the system operation and can not be controlled. The system has 7 equations and 10 variables. In this case, a parameter sweep can be performed in duty cycle D_c, and by defining two variables, like as, A_2 and A_3, the system can be solved. By varying D_c, the system can be solved and the soft-switching conditions can be ensured for any operating point.

In order to calculate Q_L, the output voltage must be considered. The DC output voltage is equal to the average value of the capacitor C_2 voltage. In this case, the fourth term on (17) should be evaluated as:

$$\frac{V_o}{V_{in}} = \frac{1}{2\pi}\int_0^{2\pi} \mathbf{y_4}(\omega t)d\omega t. \tag{35}$$

The solution of (35) is dependent of Q_L and a constant C. This allows the following relationships by considering $S = 1/\sqrt{a}$:

$$\frac{V_o}{V_{in}} = \frac{1}{2\pi}\int_0^{2\pi} \mathbf{y_4}(\omega t)d\omega t \iff \frac{V_o}{V_{in}} = CQ_L \iff \frac{1}{a\sqrt{a}} = CQ_L, \tag{36}$$

which leads to

$$Q_L = \frac{1}{a\sqrt{a}C}. \tag{37}$$

In order to show the theoretical results for the Class E^2 resonant DC/DC converter, an algorithm was implemented in a mathematical software aiming to find the state-space model solutions for any operating point. In addition, maximum values on the switches can be calculated and normalized gain and component stress curves can be obtained. Furthermore, by solving the output equation, the normalized steady-state waveforms are obtained as shown in Figure 5. The waveforms considering duty cycle, 0.4, 0.5, 0.6 and 0.7 are depicted in Figures 5.a-5.f, Figures 5.g-5.l, Figures 5.m-5.r and Figures 5.s-5.x, respectively. It can been seen that the switch S ZVS condition is ensured for all considered values of D_c as shown in Figures 5.c,5.i, 5.o, 5.u. The diode D ZDVS condition is achieved as depicted in Figures 5.d, 5.j, 5.p, 5.v.

The main normalized and component stress curves are shown in Figure 6.

III. DESIGN METHODOLOGY

In this section, a design methodology is proposed for the Class-E^2 converter. A step-by-step procedure is going to be performed.

A. Step 1: Select the operating point

The normalized gain and component stress curves depicted in Figure 6, represent the behavior of the converter. For instance, if the application requires a higher current gain, it can be necessary to use duty cycle less than 0.5, as shown in Figure 6.a. However, the lower the duty cycle, the greater the component stress, as portrayed in Figures 6.e-6.h.

Aiming to clarify the design methodology, some normalized results depicted in Figure 6 are shown in Table I.

TABLE I
Design Parameters for the Class-E^2 Resonant Converter

$A_2 = 0.75$ $A_3 = 1.25$						
D_c	T_1	T_2	A_1	Q_L	S	a
0.30	0.059	4.319	0.724	0.069	4.154	0.057
0.35	0.222	4.393	0.758	0.086	3.147	0.100
0.40	0.375	4.467	0.804	0.106	2.441	0.167
0.45	0.520	4.542	0.865	0.128	1.933	0.267
0.50	0.659	4.620	0.946	0.152	1.557	0.412
0.55	0.791	4.700	1.055	0.179	1.272	0.617
0.60	0.920	4.783	1.203	0.210	1.050	0.906
0.65	1.045	4.868	1.406	0.247	0.872	1.314
0.70	1.166	4.955	1.698	0.291	0.724	1.903
0.75	1.284	5.035	2.135	0.347	0.599	2.784
0.80	1.397	5.042	2.854	0.424	0.490	4.153

B. Step 2: Define specifications

The second step to design the converter based on the previously theoretical results is to define specifications, such as: output voltage V_o, operating frequency f and output power P_o. Based on that, the operating angular frequency ω, the output current I_o, the input current I_{in}, input voltage V_{in} and the load R_L are calculated by: $\omega = 2\pi f$, $I_o = P_o/V_o$, $I_{in} = I_o/S$, $V_{in} = P_o/I_{in}$ and $R_L = V_o/I_o$.

C. Step 3: Design of the resonant circuit

The designing equations for resonant circuit composed by C_1, L_r, C_r and C_2 can be derived from (26), (27) and (28). The

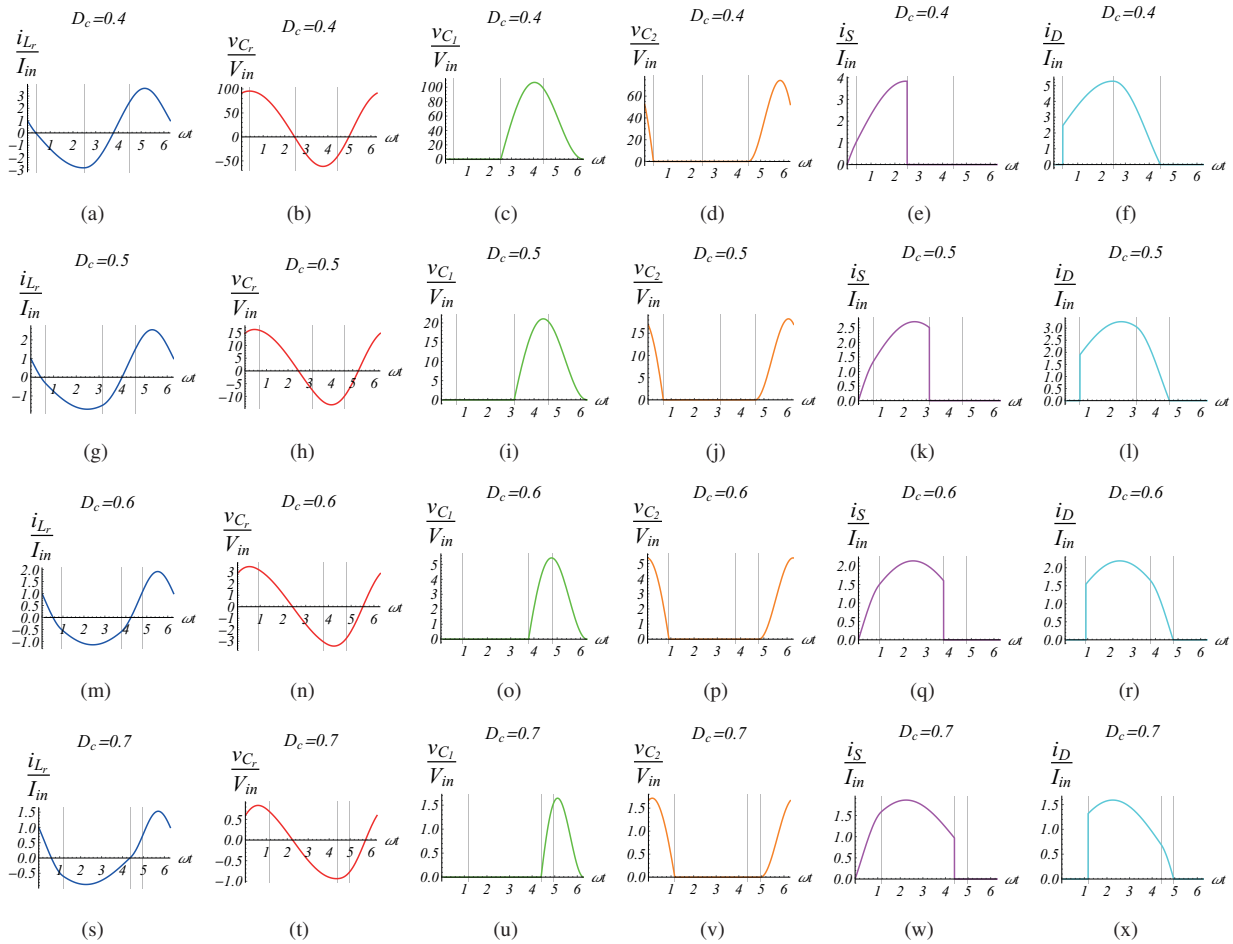

Fig. 5. Normalized waveforms for the Class-E^2 resonant converter considering $A_2 = 0.75$ and $A_3 = 1.25$. (a)-(f) $D_c = 0.4$. (g)-(l) $D_c = 0.5$. (m)-(r) $D_c = 0.6$. (s)-(x) $D_c = 0.7$.

following equations are used:

$$C_1 = \frac{A_3 Q_L}{{A_1}^2 R_L \omega}, \tag{38}$$

$$L_r = \frac{R_L}{A_3 Q_L \omega}, \tag{39}$$

$$C_r = \frac{A_3 Q_L}{{A_2}^2 R_L \omega} \tag{40}$$

and

$$C_2 = \frac{Q_L}{A_3 R_L \omega}. \tag{41}$$

D. Step 4: Design of the choke inductor and output filter

The choke inductor L_c can be designed by defining a normalized resonant frequency A_c between L_c and C_1 as follows:

$$A_c = \frac{\omega_c}{\omega}, \tag{42}$$

in which, the angular frequency is $\omega_c = 1/\sqrt{L_c C_1}$. The lower A_c, the lower the ripple in the choke inductor L_c, which is calculated as

$$L_c = \frac{{A_1}^2 R_L}{A_c Q_L \omega}. \tag{43}$$

The output filter inductor L_f can be designed in the same way as L_c, by considering a normalized resonant frequency A_f between L_f and C_f:

$$A_f = \frac{\omega_f}{\omega}, \tag{44}$$

being $\omega_f = 1/\sqrt{L_f C_f}$. The equation for L_f is dependent of T_1 and T_2:

$$L_f = \frac{(1 - T2 + T1) R_L}{A_f \omega}. \tag{45}$$

Finally, the output filter capacitor C_f is designed as [1]

$$C_f = \frac{25}{\omega^2 L_f}. \tag{46}$$

IV. RESULTS

This section shows a comparison among theoretical, simulation and experimental results. Let us consider a step-down low-power application that requires an output voltage of $4\,V$, output power of $800\,mW$ and operating frequency of $800\,kHz$. It can be seen in the design abacus in Figure 6.a and Figures 6.e-6.h that for duty cycle 0.5, a reasonable current transfer function and component stresses are achieved. By selecting $D_c = 0.5$, the unit-less parameters are extracted from

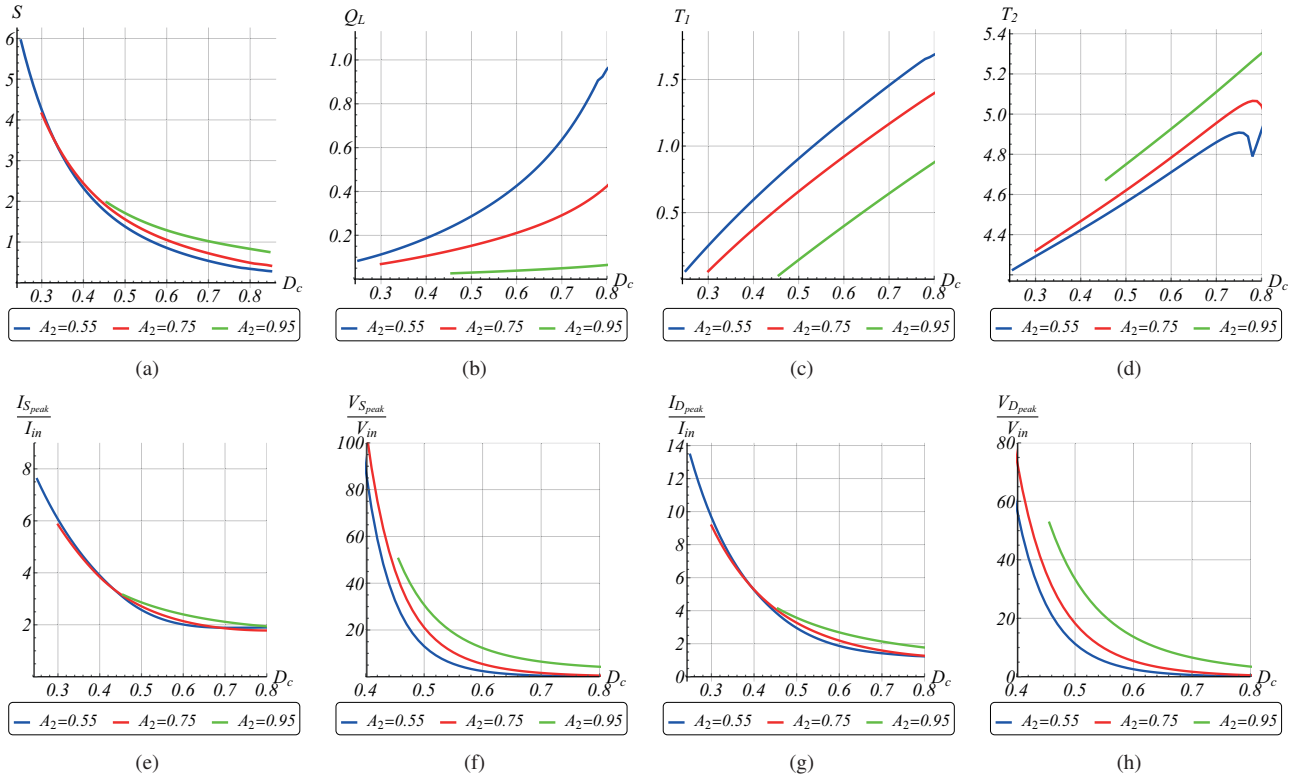

Fig. 6. Normalized gain and component stress curves as function of duty cycle D_c for the Class-E^2 resonant converter considering $A_3 = 1.25$. (a) Current transfer function, S. (b) Quality factor, Q_L. (c) Diode D turn-on, T_1. (d) Diode D turn-off, T_2. (e) Switch S peak current, $I_{S_{peak}}/I_{in}$. (f) Switch S peak voltage, $V_{S_{peak}}/V_{in}$. (g) Diode D peak current, $I_{D_{peak}}$ (h) Diode D peak voltage, $V_{D_{peak}}$.

the design abacus and are described in Table I. The output current and the required input current are calculated in Step 2 of Section III. The converter components are designed by (38), (39), (40), (41), (43), (45) and (46). The specifications, selected operating point and designed components are shown in Table III. The converter was assembled for the experimental results. The results are shown in Figure 7. The simulation results were obtained from SPICE software and the theoretical results from a mathematical software. The soft-switching conditions were achieved. A quantitative comparison among theoretical, simulation and experimental results is going to be performed in order to analyze the error. The error analysis is shown in Table II. For the analysis the choke inductor and the output filter were replaced by constant current sources. This assumption leads to a restriction on the method, which is related to the possible values for A_c and A_f. These values can not be close to A_1, A_2 and A_3 in order to ensure that L_c, L_f and C_f do not affect the behavior of the resonant circuit.

TABLE II
Error Analysis

Peak value	Theoretical	Simulation	Experimental	Error
i_{L_r}	$0.370A$	$0.370A$	$0.360A$	2.7%
v_S	$23.4A$	$23.4V$	$22.9V$	2.2%
v_{C_2}	$20A$	$19.8V$	$22V$	9.0%
V_o	$4V$	$4.05V$	$4.15V$	3.6%

TABLE III
Specifications and Designed Components

Specifications / Components	Value
Duty cycle, D_c	0.5
Operating frequency, f	$800\,kHz$
Output voltage, V_o	$4V$
Output power, P_o	$800\,mW$
Output current, I_o	$200\,mA$
Input current, I_{in}	$128\,mA$
Current transfer function, S	1.557
Normalized resonant frequency, A_1	0.94
Normalized resonant frequency, A_2	0.75
Normalized resonant frequency, A_3	1.25
Choke inductor ripple as a normalized resonant frequency, A_c	0.09
Output ripple as a normalized resonant frequency, A_f	0.1
Diode turn-on time, T_1	0.659
Diode turn-off time, T_2	4.620
Resonant inductor, L_r	$22\mu H$
Resonant capacitor, C_r	$3.3\,nF$
Capacitor, C_1	$2.2\,nF$
Capacitor, C_2	$1.2\,nF$
Choke inductor, L_c	$260\,\mu H$
Output filter inductor, L_f	$175\,\mu H$
Output filter capacitor, C_f	$25\,nF$
Load, R_L	$20\,\Omega$

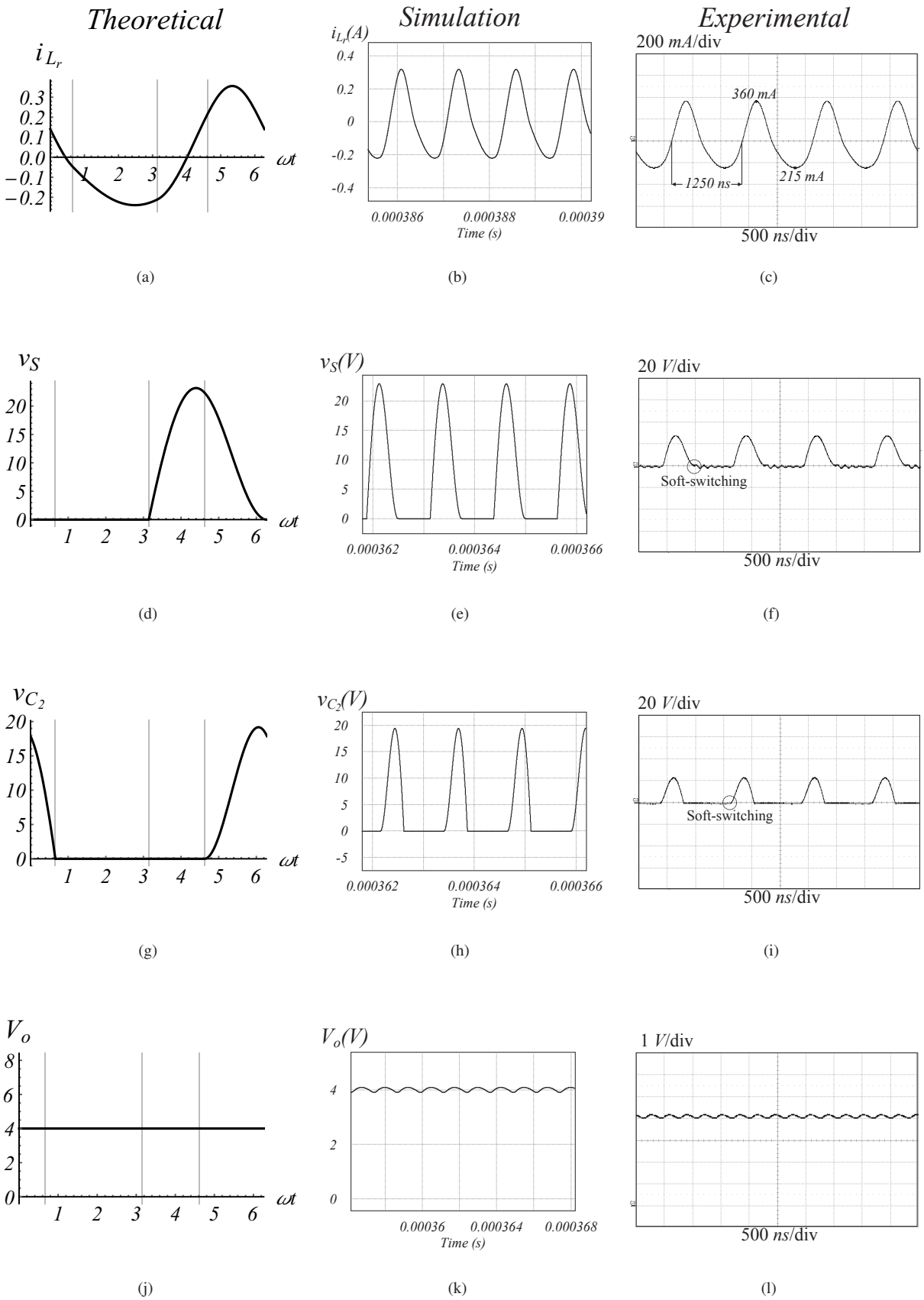

Fig. 7. Results. (a)-(c) Inductor L_r current. (d)-(f) Switch S voltage. (g)-(i) Capacitor C_2 voltage. (j)-(l) Output voltage.

V. CONCLUSION

A steady-state analysis and design methodology for Class-E^2 resonant DC/DC converters were presented in this work. This was the first state-space representation for such combination of a Class-E inverter and a Class-E rectifier. The proposed model is independent of specifications and real system components, which allows to obtain analytical waveforms and normalized gain and component stress curves. The state-space model allows to solve all operating modes. Subsequently, a linear system that includes steady-state and soft-switching conditions can be evaluated. The Class-E^2 converter was assembled based on a proposed design methodology. The method can be used to analyze resonant DC/DC converters without separating the inverter to the rectifier stage. In contrast, the proposed method is more complex than other works. In this sense, it is concluded that a trade-off between complexity and accuracy should be taken into account. For second order PWM DC/DC converters, standard methods can achieve the same accuracy of the proposed method in a simpler way. However, for resonant converters, the proposed method is suitable because it can predict the soft-switching operation for a wide operation range. Experimental and simulations results have shown agreement with the mathematical approach.

APPENDIX - NORMALIZED STATE-SPACE MODEL INCLUDING DIODE VOLTAGE DROP

For low voltage levels, the diode D voltage drop V_D plays a significant role. In this sense, this section shows te normalized state-space model for the Class-E^2 resonant DC/DC converter. In this case, the state-space models for operating modes II and III, in which the diode D is off, are going to be enhanced in order to consider the diode voltage drop. The operating modes II and III including the model for the diode voltage drop are depicted in Figure 8.a Figure 8.b.

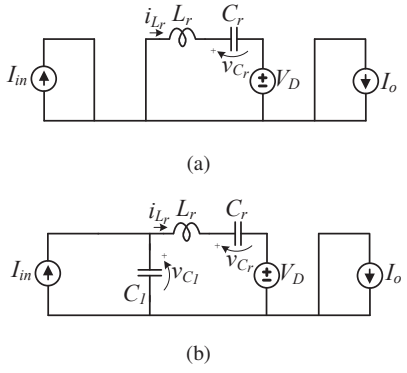

Fig. 8. Operating modes including model for the diode voltage drop. (a) Switch S on and diode D on. (b) Switch S off and diode D on.

This leads to a third input for the system, which is the diode voltage drop V_D. The input vector becomes:

$$\mathbf{u}(t) = [\mathbf{I_{in}}, \mathbf{I_o}, \mathbf{V_D}]^T. \tag{47}$$

By following the proposed methodology, the input vector is normalized by the input source I_{in}, which leads to:

$$\mathbf{u}(\omega t) = \left[\frac{\mathbf{I_{in}}}{\mathbf{I_{in}}}, \frac{\mathbf{I_o}}{\mathbf{I_{in}}}, \frac{\mathbf{V_D}}{\mathbf{V_{in}}}\right]^T = \left[1, S, Q_L\frac{V_D}{V_{in}}\right]^T = \left[1, \frac{1}{\sqrt{a}}, Q_L U\right]^T, \tag{48}$$

in which, U is the diode voltage drop normalized by the input source. The resulting normalized state-space model is described by the following matrices:

$$\mathbf{E}_I = \begin{bmatrix} 0 & -A_2 & 0 & -A_3 \\ A_2 & 0 & 0 & 0 \\ 0 & 0 & 0 & 0 \\ A_3 & 0 & 0 & 0 \end{bmatrix}, \quad \mathbf{F}_I = \begin{bmatrix} 0 & 0 & 0 \\ 0 & 0 & 0 \\ 0 & 0 & 0 \\ 0 & -1 & 0 \end{bmatrix},$$

$$\mathbf{E}_{II} = \begin{bmatrix} 0 & -A_2 & 0 & 0 \\ A_2 & 0 & 0 & 0 \\ 0 & 0 & 0 & 0 \\ 0 & 0 & 0 & 0 \end{bmatrix}, \quad \mathbf{F}_{II} = \begin{bmatrix} 0 & 0 & -1 \\ 0 & 0 & 0 \\ 0 & 0 & 0 \\ 0 & 0 & 0 \end{bmatrix},$$

$$\mathbf{E}_{III} = \begin{bmatrix} 0 & -A_2 & A_1 & 0 \\ A_2 & 0 & 0 & 0 \\ -A_1 & 0 & 0 & 0 \\ 0 & 0 & 0 & 0 \end{bmatrix}, \quad \mathbf{F}_{III} = \begin{bmatrix} 0 & 0 & -1 \\ 0 & 0 & 0 \\ \frac{A_1}{A_3} & 0 & 0 \\ 0 & 0 & 0 \end{bmatrix},$$

$$\mathbf{E}_{IV} = \begin{bmatrix} 0 & -A_2 & A_1 & -A_3 \\ A_2 & 0 & 0 & 0 \\ -A_1 & 0 & 0 & 0 \\ A_3 & 0 & 0 & 0 \end{bmatrix} \text{ and } \mathbf{F}_{IV} = \begin{bmatrix} 0 & 0 & 0 \\ \frac{A_1}{A_3} & 0 & 0 \\ 0 & 0 & 0 \\ 0 & -1 & 0 \end{bmatrix}.$$

ACKNOWLEDGEMENTS

This study was financed in part by the Coordenação de Aperfeiçoamento de Pessoal de Nível Superior - Brasil (CAPES/PROEX) - Finance Code 001 and by the National Council for Scientific and Technological Development - CNPq(315101/2018-0).

REFERENCES

[1] M. K. Kazimierczuk, D. Czarkowski, "Resonant Power Converters", *John Wiley & Sons, Inc.*, 1995.

[2] M. Liu, Y. Qiao, S. Liu, C. Ma, "Analysis and Design of A Robust Class E^2 DC-DC converter for Megahertz Wireless Power Transfer", *IEEE Trans. Power Electron.*, vol. 32, pp. 2835-2845, May. 2016.

[3] N. F. O. Da Silva, M. L. Heldwein, A. J. Perin, "Conversor Wireless com Retificador ZCS", *Revista Eletrônica de Potência*, vol. 22, no. 3, pp. 298-309, Set. 2017.

[4] C. Cheng, Z. Zhou, W. Li, C. Zhu, Z. Deng, C. Mi, "Analysis and Design of A Robust Class E^2 DC-DC converter for Megahertz Wireless Power Transfer", *IEEE Trans. Power Electron.*, vol. 32, pp. 2835-2845, May. 2016.

[5] A. Tanaka, F. Utsunomiya, T. Douseki, "Wearable Self-Powered Diaper-Shaped Urinary-Incontinence Sensor Suppressing Response-Time Variation with 0.3-V Start-Up Converter", *2014 IEEE SENSORS*, pp. 103-117, Nov. 2014.

[6] R. La Rosa, P. Livreri, C. Trigona, L. Di Donato, G. Sorbello, "Strategies and Techniques for Powering Wireless Sensor through Energy Harvesting and Wireless Power Transfer", *sensors*, vol. 19, pp. 1-16, Jun. 2019.

[7] F. Meddour, Z. Dibi, “An Efficient Small Size Electromagnetic Energy Harvesting Sensor for Low-DC-power Applications", *IET Microwaves, Antennas & Propagation*, vol. 11, pp. 483-489, Apr. 2017.

[8] D. R. Rodrigues, “A MCU based DC-DC Step-Up Converter Providing Regulation of its Own Power Supply", *2015 IEEE 13th Brazilian Power Electronics Conference and 1st Southern Power Electronics Conference (COBEP/SPEC)*, pp. 1-4, Nov. 2015.

[9] M. Khanna, “Design of DC-DC Converters using Tunable Piezoelectric Transformers", *Master‘s Dissertation*, 2017.

[10] M. Khanna, R. Burgos, Q. Wang, K. Ngo, A. Carazo, “New Tunable Piezoelectric Transformers and Their Application in DC-DC Converters", *IEEE Transactions on Power Electronics*, vol. 32, pp. 8974-8978, May 2017.

[11] N. González-Santini, H. Zeng, Y. Yu, F. Peng, “Z-Source Resonant Converter With Power Factor Correction for Wireless Power Transfer Applications", *IEEE Transactions on Power Electronics*, vol. 31, pp. 7691-7700, Apr. 2016.

[12] T. Nagashima, X. Wei, E. Bou, E. Alarcón, M. K. Kazimierczuk, H. Sekiya, “Analysis and Design of Loosely Inductive Coupled Wireless Power Transfer System Based on Class-E^2 DC-DC Converter for Efficiency Enhancement", *IEEE Trans. on Circuit and Systems I: Regular Papers*, vol. 62, pp. 2781-2791, Nov. 2015.

[13] D. C. Pereira, P. L. Tavares, P. S. Almeida, G. M. Soares, F. L. Tofoli, H. A. C. Braga, “Improved Photoelectrothermal Model with Thermal Parameters Variation Applied to an Extra-High Current COB LED", *Revista Eletrônica de Potência*, Jun. 2019.

[14] C. R. B. S. Rodrigues, P. S. Alem, P. S. Almeida, G. M. Soares, M. F. Braga, H. A. C. Braga, “A Novel Linear Circuit for Current Equalization In LED Strings", *Revista Eletrônica de Potência*, vol. 18, no. 3, Aug. 2013.

[15] T. Nagashima, X. Wei, E. Bou, E. Alarcón, M. K. Kazimierczuk, H. Sekiya, “Steady-State Analysis of Isolated Class-E^2 Converter Outside Nominal Operation", *IEEE Transactions on Industrial Electronics*, vol. 64, pp. 3227-3238, Nov. 2016.

[16] N. Dal Pont, D. Junior, T. Lazzarin, I. Barbi, “Conversor CC-CC Paralelo Ressonante Meia Ponte Assim´etrico com Sa´ida em Tensão", *Revista Eletrônica de Potência*, vol. 23, no. 1, pp. 108-117, Mar. 2018.

[17] M. Ponce, J. Arau, R. Osorio, M. Juarez, M. Álvarez, “A Novel High-Power-Factor Single-Switch Electronic Ballast for Compact Fluorescent Lamps", *Revista Eletrônica de Potência*, vol. 09, no. 1, pp. 63-70, Jun. 2004.

[18] L. Vilefort, F. Silva, E. Coelho, L. Freitas, J. Júnior, “Amplificador Classe D de Potência Alimentado com Fonte de Tensão CC Simples ou Simétrica", *Revista Eletrônica de Potência*, vol. 15, no. 3, pp. 158-165, Aug. 2010.

[19] I. Barbi, “Conversores Estáticos CC-CC com Comutação Suave", *Revista Eletrônica de Potência*, vol. 02, no. 1, pp. 1-12, Jun. 1997.

[20] L. S. Mendonça, Thiago. C. Naidon, G. G. Freitas, M. L. S. Martins, F. E. Bisogno, “Energy-Based Normalization for Resonant Power Converters", *IEEE Transactions on Power Electronics*, vol. 33, pp. 6526-6536, Aug. 2018.

[21] M. K. Kazimierczuk, W. Szaraniec, “Class D-E Resonant DC/DC Converter", *IEEE Trans. on Aerospace and Electronic Systems*, vol. 29, pp. 963-976, Jul. 1993.

[22] Y. Guan, Y. Wang, W. Wang, D. Xu, “Analysis and Design of a High-Frequency DC/DC Converter Based on a Resonant Rectifier", *IEEE Trans. Ind. Electronics*, vol. 64, pp. 8492-8503, Apr. 2017.

[23] Y. Huang, N. Shinohara, T. Mitani, “Impedance Matching in Power Transfer", *IEEE Transactions on Microwave Theory and Techniques*, vol. 65, pp. 582-590, Feb. 2017.

[24] F. E. Bisogno, “Energy-related System Normalization and Decomposition Targeting Sensitivity Consideration", *PhD Dissertation*, Fakultät für Elektrotechnik und Informationstechnik der Technischen Universität Chemnitz-Zwickau, Jun. 2006.

[25] L. S. Mendonça, F. E. Bisogno, “Resonance-Based Normalization Theory for Analysis and Design of Resonant Power Converters", *Revista Eletrônica de Potência*, vol. 24, no. 3, Set. 2019.

BIOGRAPHIES

Lucas S. Mendonça, is a control and automation engineer (2015) and master in Electrical Engineering (2017) with the Universidade Federal de Santa Maria, Brazil. He is currently a double degree doctorate candidate with the Universidade Federal de Santa Maria and the Brandenburg University of Technology Cottbus-Senftenberg, Germany. His areas of interest are: power electronics and contactless energy transfer systems.

João Pedro S. Cipriani, received the B.Sc. degree in Electrical Engineering (2019) from the Universidade Federal de Santa Maria, Brazil. He has been with the Electrical and Computational Systems Research and Development Group (GSEC) since 2015, where he is currently working towards his Master Degree. His research interests include smart drivers for lighting, energy harvesting and battery charging devices.

Thiago C. Naidon, is an electrical engineer (2012) and master in Electrical Engineering (2015) with the Universidade Federal de Santa Maria, Brazil. He was professor at Universidade Tecnológica Federal do Paraná from 2017 to 2019. He is currently a professor at Universidade Federal de Santa Maria at Colégio Técnico Industrial de Santa Maria. His areas of interest are: power electronics and energy harvesting.

Fábio E. Bisogno, is an electrical engineer (1999), master (2001) with the Universidade Federal de Santa Maria and Dr.-Ing. in Electrical Engineering (2006) with the Technische Universität Chemnitz, Germany. He is currently a full professor at Universidade Federal de Santa Maria. His areas of interest are: resonant converters and self-oscillating systems.